Preliminary Report on TRMM-LBA Rainfall Estimation Using the S-POL Radar

by
L.D. Carey, R. Cifelli, W.A. Petersen, and S.A. Rutledge

Department of Atmospheric Science
Colorado State University
Fort Collins, Colorado

Colorado
State
University

Department of
Atmospheric Science

Paper No. 697

PRELIMINARY REPORT ON

TRMM-LBA RAINFALL ESTIMATION USING THE S-POL RADAR

by

Lawrence D. Carey

Robert Cifelli

Walter A. Petersen

Steven A. Rutledge

Department of Atmospheric Science

Colorado State University

Fort Collins, CO 80523

October 27, 2000

Atmospheric Science Paper No. 697
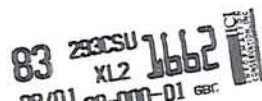
Preliminary Report on

TRMM[1]-LBA Rainfall Estimation Using the S-POL Radar

L. D. Carey[2], R. Cifelli, W. A. Petersen, and S. A. Rutledge

Radar Meteorology Group
Department of Atmospheric Science
Colorado State University
Fort Collins, CO 80523

October 27, 2000

[2] Corresponding author e-mail: carey@atmos.colostate.edu

1. Introduction

By measuring the returned power and phase at both horizontal and vertical polarizations, polarimetric radars provide information on the drop size distribution, shape, orientation, and thermodynamic phase of hydrometeors. As a result, polarization radar techniques afford a more accurate estimate of rainfall than conventional reflectivity-based radar methods (Zrnic and Ryzhkov, 1999). The presence of the NCAR S-POL radar (10.7 cm, polarimetric) during the LBA (Large Scale Biosphere-Atmosphere) field campaign in Rondonia, Brazil provides the TRMM (Tropical Rainfall Measuring Mission) validation community with an unprecedented opportunity to accurately estimate rainfall over a large domain (O 10,000 km^2) in a tropical continental locale.

This report summarizes preliminary progress toward the estimation of rainfall with the S-POL radar during the LBA field campaign. In Sec. 2, we highlight key elements of our data processing and rainfall analysis methodology. In Sec. 3, we describe the available Version 1 (V1) S-POL rainfall products. We then present a simple comparison between V1 S-POL radar and gauge rainfall accumulations. In Sec. 4, we summarize some key scientific results to date. Finally, we discuss our Version 2 (V2) strategy for improving the S-POL rainfall estimate and plans for scientific applications of this data. The S-POL radar V1 rainfall products and a more comprehensive description of our TRMM-LBA research can be found at http://radarmet.atmos.colostate.edu/trmm_lba/.

2. Methodology

a. Data Processing

The raw S-POL data suffers from the presence of clear-air echo, ground clutter, anomalous propagation, second-trip echoes, partial beam blocking, precipitation attenuation, calibration biases, and gaseous attenuation. Many of these deleterious effects can be readily seen in the low-level PPI summaries provided by NCAR ATD at http://www.atd.ucar.edu/rsf/TRMM-LBA/trmm_intro.htm. Polarization radar data allow novel approaches to the mitigation of all these problems except the last. For gaseous attenuation, we apply a simple range correction using an assumed correction coefficient.

As shown by Ryzhkov and Zrnic (1998), thresholds in the correlation coefficient (ρ_{hv}) and the variance of the differential phase (ϕ_{dp}) can be used to remove the majority of non-meteorological, clear-air returns, ground clutter, second-trip echoes, and anomalous propagation. Based on statistical analyses of the data, we characterized any echo with $\rho_{hv} > 0.8$ and $\sigma(\Phi_{dp}) < 12°$ as hydrometeors. All other echoes were removed. Additional clear air echo was identified and removed by searching for anti-correlated pairs of very large Z_{dr} and small Z_h. If $Z_h < 35$ dBZ and $Z_{dr} > Z_{drca}(Z_h)$, then the range gate was identified as clear air and removed where Z_{dr} "clear air" is defined as:

$$Z_{drca}(Z_h) = 2 \ dB \qquad\qquad if \ Z_h < 0 \ dBZ$$
$$= 0.2 \circ Z_h + 2 \ dB \qquad if \ 0 \leq Z_h \leq 15 \ dBZ$$
$$= 5 \ dB \qquad\qquad\quad if \ 15 < Z_h < 35 \ dBZ$$

2

We then filtered the measured differential phase and estimated the specific differential phase (K_{dp}) according to the procedures outlined in Hubbert and Bringi (1995).

Frequent vertical pointing scans during LBA demonstrated that there was little or no absolute bias ($|Z_{drbias}| < 0.1$ dB) in the differential reflectivity (Z_{dr}). For more information, reference the analyses and discussion by Mr. Bob Rilling (NCAR-ATD) at the following web site, http://www.atd.ucar.edu/rsf/TRMM-LBA/quicklook/qa/trmm_zdr_bias.html. As detailed by Scarchilli et al. (1996), internal consistency between observations of the horizontal reflectivity (Z_h), the differential reflectivity (Z_{dr}), and the specific differential phase (K_{dp}) can be used to estimate a calibration offset in Z_h if the relative bias in Z_{dr} is known. In this method, K_{dp} is estimated from measurements of Z_h and Z_{dr} as determined by a theoretical relationship. This estimated K_{dp} is then compared to the measured K_{dp}. The offset in Z_h is varied until the match between estimated and observed K_{dp} is optimized. Utilizing this procedure, we determined that Z_h was biased by about -0.8 dB (biased 0.8 dB low, see Fig. 1). Dr. Steve Bolen of CSU/EE and Mr. Scott Ellis and Dr. J. Vivekanandan of NCAR (personal communication, 2000) obtained similar bias results in the range of -0.3 to -0.75 dB. Since there is some uncertainty in this methodology (e.g., assumed drop shape) and since the absolute bias was small ($|Z_{hbias}| < 1$ dB, we chose not to apply an engineering bias correction to the Z_h data.
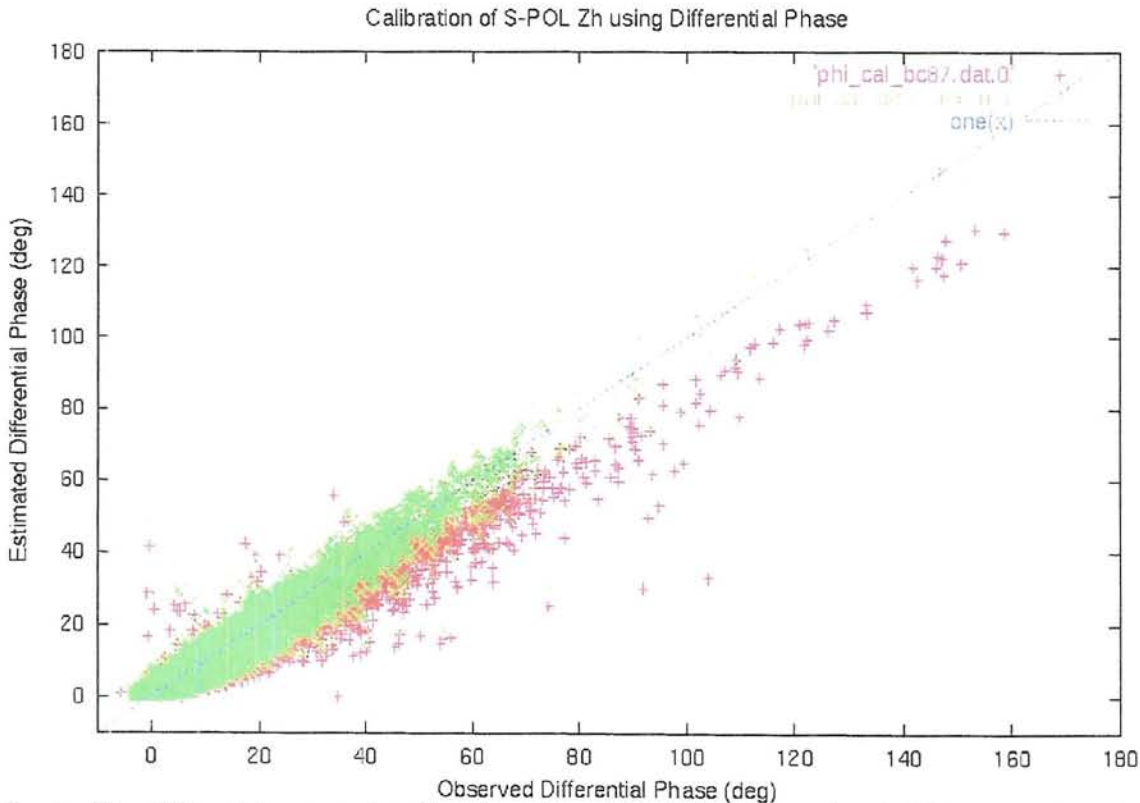

Fig. 1. The differential propagation phase is estimated from the horizontal and differential reflectivity and then plotted against the observed differential propagation phase. The red +'s are prior to any bias correction and the green \'s are after a -0.8 dB correction is applied to the horizontal reflectivity.

a.

'zh_phidp.dat'

zh(x)=-0.0145*x+47.75

b.

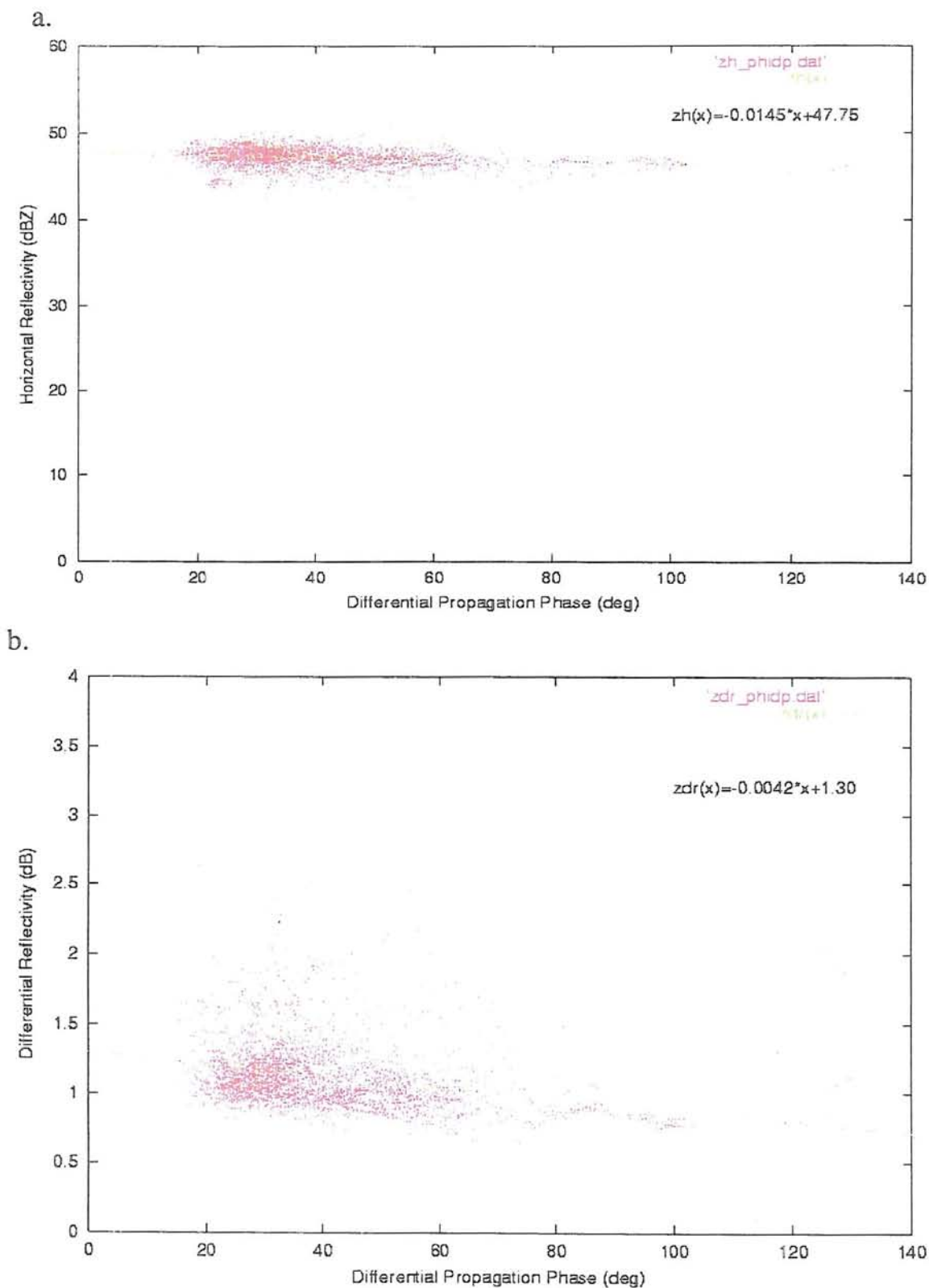'zdr_phidp.dat'

zdr(x)=-0.0042*x+1.30

Fig. 2. Trend of the (a) horizontal reflectivity and (b) differential reflectivity with the differential propagation phase. The slope of the line in a (b) is the negative of the correction coefficient for horizontal (differential) attenuation. See Carey et al. (2000) for a detailed explanation of the propagation correction procedure. For these plots, we isolated points from 80 hours of data that satisfied $2 \leq K_{dp} \leq 3°$ km^{-1}.

To correct for propagation effects caused by precipitation at S-band, we used the procedure outlined by Bringi et al. (1990), Ryzhkov and Zrnic (1995a), and Carey et al. (2000). As seen in Figs. 2a,b, horizontal (differential) attenuation correction coefficients can be obtained by analyzing the trend of Z_h (Z_{dr}) with ϕ_{dp}. We obtained the correction coefficients a=0.0145 and b = 0.0042 and applied them according to Carey et al. (2000).
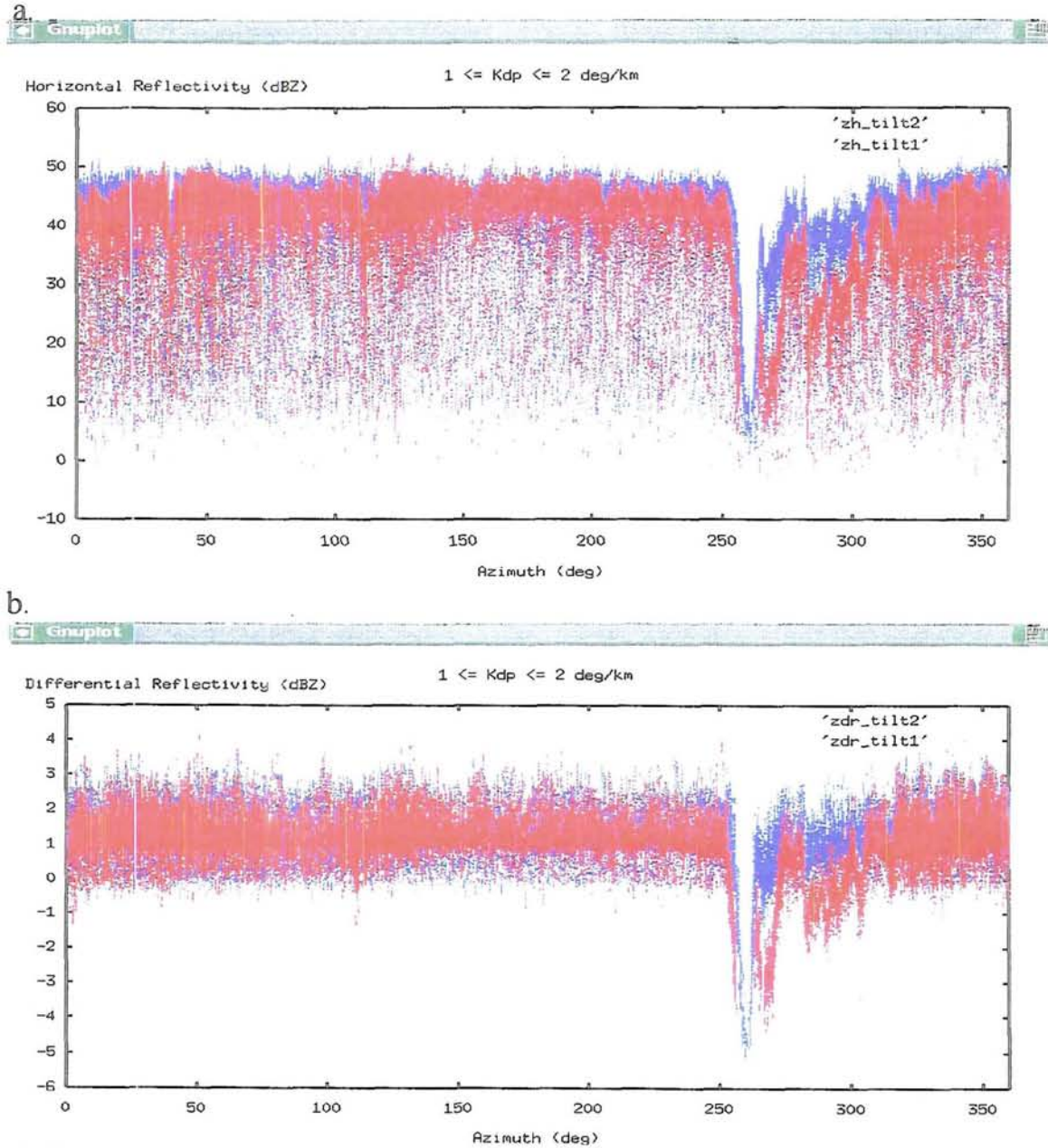

Fig. 3. Plot of the (a) horizontal reflectivity and (b) differential reflectivity as a function of azimuth. The red (blue) points are from the 1st (2nd) tilt of a series of low-level PPI's over 80 hours during twelve different case days for which $1 \leq K_{dp} \leq 2°$ km[-1].

We also identified areas adversely affected by partial (and occasionally complete) blocking by analyzing the azimuthal trend of Z_h and Z_{dr} that satisfied $1 \leq K_{dp} \leq 2°$ km[-1]. Independent of

blocking effects, this threshold in K_{dp} should result in a fixed range of Z_h and Z_{dr} values (as determined by drop size distribution characteristics and measurement error). As seen in Figs. 3ab, blocking effects are readily apparent in these plots.

Note the severe partial (and occasional complete) blocking effects evident in Figs. 3ab from about 250° to 315° in azimuth (i.e., from WSW to NW). To avoid biasing V1 rainfall estimates, the differential reflectivity was masked out of regions with significant blocking and the horizontal reflectivity was corrected by adding a fixed dB offset as a function of range (see Fig. 4) if the correction exceeded 1 dB. If the inferred correction to Z_h exceeded 35 dB, then no correction was applied and Z_h in those rays were set to the bad data flag.
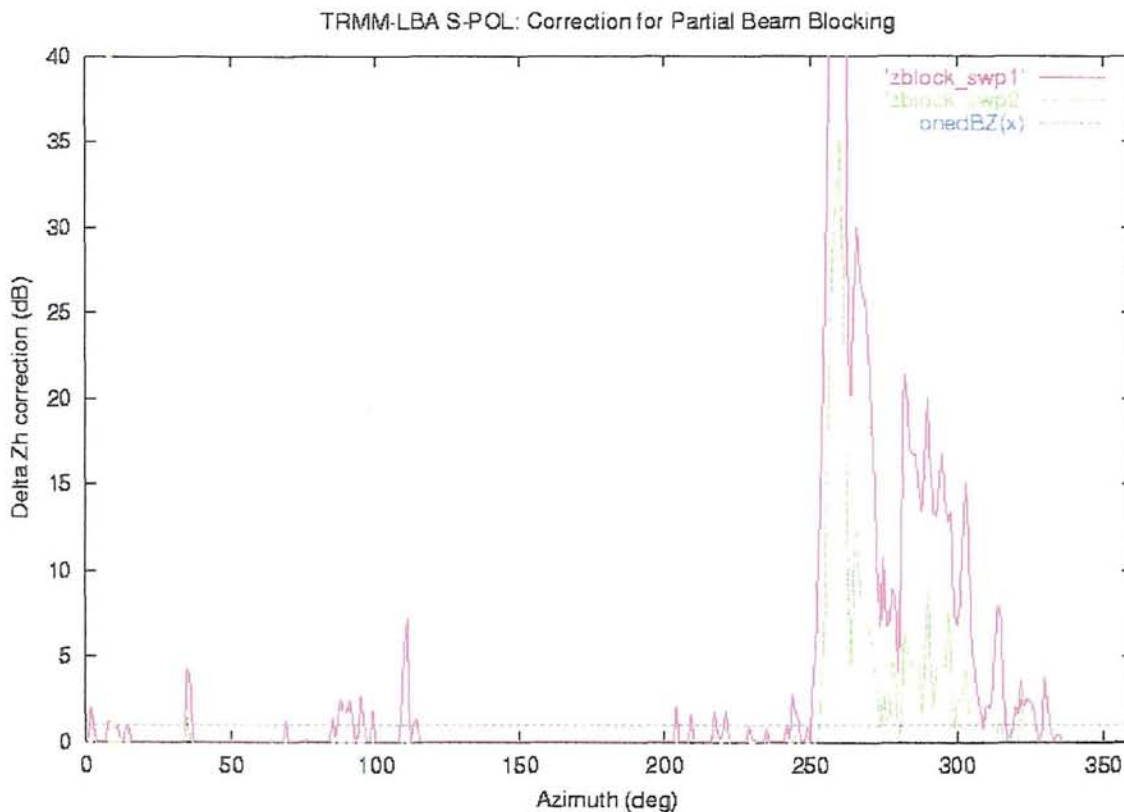

Fig. 4. This plot represents the ΔZ_h correction (dB) for partial blocking as a function of azimuth for the first (red) and second (green) tilts. For V1 processing, the correction was added if it exceeded 1 dB and was less than 35 dB. If ΔZ_h correction > 35 dB, the horizontal reflectivity was not corrected but was set to the bad data flag. If ΔZ_h correction < 1 dB, no correction was made.

The above steps were accomplished in Universal Format (UF) using FORTRAN code written by Dr. Lawrence D. Carey and Mr. Paul Hein of CSU Radar Meteorology. The resulting processed data set was output in UF out to a range of 100 km from the S-POL radar and up to a height of 3.5 km AGL in order to minimize beam spreading and contamination by melting hydrometeors. For rainfall maps, we utilized processed UF data from full 360° surveillance scans only, which typically consisted of only 2 low-level tilts at elevation angles of about 0.7° and 1.1°. The surveillance scans were available approximately every ten minutes. Using the REORDER software package, these scans were interpolated to a 100 km × 100 km horizontal Cartesian grid, centered on the S-POL radar at a height of 1 km AGL. The horizontal grid resolution is 2 km × 2

km. Radii of influence for the interpolation process were 1.0 km in the horizontal and 1.0 km in the vertical. Although rain maps are available approximately every ten minutes for the entire operational period of the S-POL radar (10 Jan 99 – 28 Feb 99), around the clock S-POL radar operations (24 hours per day, 7 days per week) began on 16 January 1999. After this time, the S-POL radar ran nearly continuously, with only short interruptions until 28 February 1999, 2213 UTC. During 24/7 operations, there were approximately 3 hours of unplanned and 8 hours of planned down time. The planned S-POL down times were always accomplished during convectively quiescent periods.

b. Rainfall Estimation

Our first efforts were aimed at making a quick estimate of areal mean rain rates over the S-POL domain. We applied the new polarimetric radar technique introduced by Ryzhkov et al. (2000) to estimate areal rainfall. The method utilizes values of the differential propagation phase, ϕ_{dp}, on the areal contour of the region of interest. In our study, a series of concentric rings in the S-POL domain out to 120 km were utilized in the areal integrals found in Ryzhkov et al. (2000). This approach minimized the error associated with assuming a mean constant rain rate in the integrated range. These data were used to analyze the time series of rainfall, the diurnal cycle of rainfall, and the distribution of areal rain rates by meteorological regime (See Sec. 3).
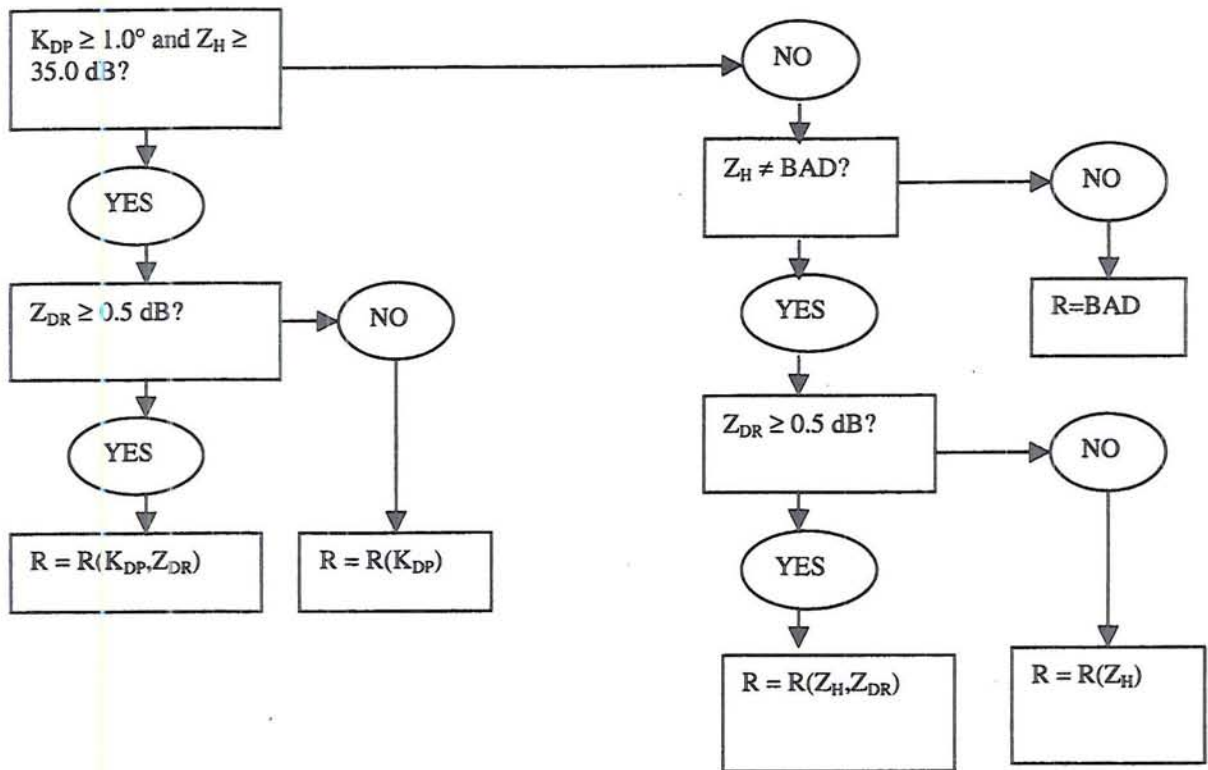
Reliable point estimates of rain rates for each radar volume were calculated using an optimization technique with the parameters Z_H, Z_{DR}, and K_{DP} (Jameson, 1991; Chandrasekar et al. 1993; Carey and Rutledge 1998; Petersen et al. 1999; Carey and Rutledge, 2000). The rain rate relation for each grid point is chosen based on thresholds in the above three polarimetric variables that minimize the rain rate standard error as described in Fig. 5. In essence, we are optimizing the rain rate relation for the given microphysical situation and radar measurement error in the above three variables at each grid point. The rain rate relations for each polarimetric radar rain rate estimator are shown in Table 1.

Table 1. Polarimetric radar rain rate estimators[*]

$$1. \ R(K_{dp}, Z_{dr}) = 87.6 \bullet \left(K_{DP}\right)^{0.934} \bullet \left(10\right)^{\left(0.1 \bullet -1.59 \bullet Z_{DR}\right)} \ \text{mm h}^{-1}$$

$$2. \ R(Z_h, Z_{dr}) = 6.70 \times 10^{-3} \bullet \left(Z_H\right)^{0.927} \bullet \left(10\right)^{\left(0.1 \bullet -3.433 \bullet Z_{DR}\right)} \ \text{mm h}^{-1}$$

$$3. \ R(K_{dp}) = 53.8 \bullet \left(K_{DP}\right)^{0.85} \ \text{mm h}^{-1}$$

$$4. \ R(Z_h) = 0.02180 \bullet \left(Z_H\right)^{0.070} \ \text{mm h}^{-1}$$

* Units: K_{dp}, $° \text{km}^{-1}$; Z_{dr}, dB; and Z_h, $\text{mm}^6 \text{m}^{-3}$. Equations (1) – (3) were taken from Bringi and Chandrasekar (2000). Equation (4) was derived from TRMM-LBA disdrometer data by Dr. Ali Tokay (personal communication, 2000)

Unblocked Beam Data

$K_{DP} \geq 1.0°$ and $Z_H \geq 35.0$ dB? → NO

NO → $Z_H \neq$ BAD? → NO → R=BAD

YES

$Z_{DR} \geq 0.5$ dB? → NO

YES (under $Z_H \neq$ BAD?)

YES → R = R(K_{DP},Z_{DR})

NO → R = R(K_{DP})

$Z_{DR} \geq 0.5$ dB? → NO

YES

R = R(Z_H,Z_{DR})

NO → R = R(Z_H)

Partially Blocked Beam Data

$K_{DP} \geq 0.25°$? → NO

YES

R = R(K_{DP})

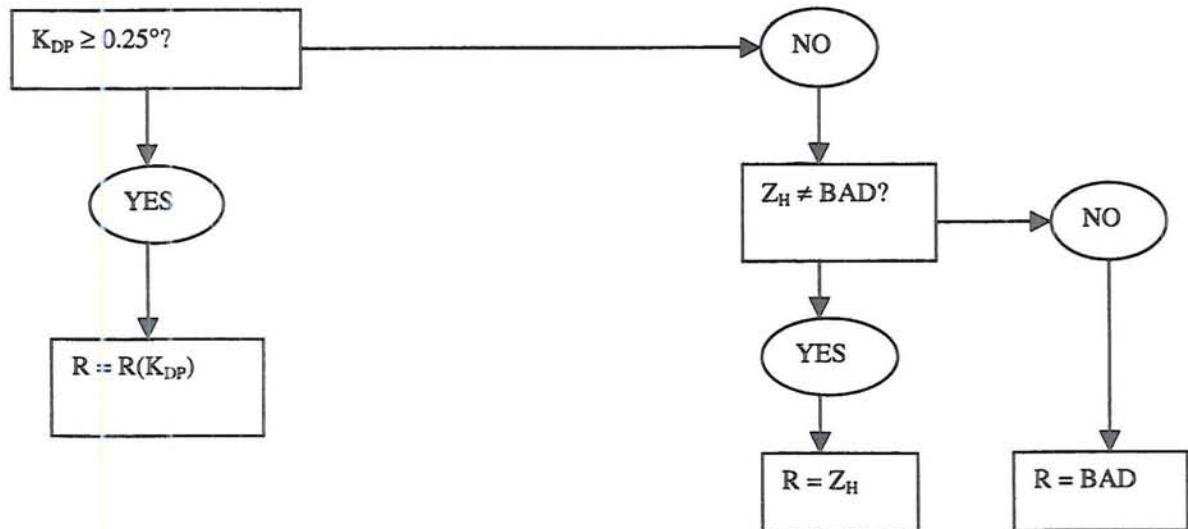NO → $Z_H \neq$ BAD? → NO

YES

R = Z_H

NO → R = BAD

Figure 5. Decision tree algorithm used to determine which polarimetric estimator is used to calculate rain rate for a specific grid point using the polarization radar optimization technique. The rain rate estimator equations are shown in Table 1.

3. Version 1 (V1) TRMM-LBA S-POL Rainfall Maps

a. Available products

Areal rain rate estimates were computed over the TRMM-LBA domain using the differential phase method of Ryzhkov et al. (2000). This effort was completed during May 2000. Since all surveillance scans were utilized, the temporal sample is typically every ten minutes or better. Selected scientific results on the diurnal cycle and the dependency of areal rainfall statistics on meteorological regime (i.e., easterly versus westerly low-level flow) are presented in Sec. 4 of this report. A nearly continuous record of areal rain rate is available from 16 Jan 99 to 28 Feb 99. For those TRMM scientists interested in these data, please contact the CSU Radar Meteorology Group for a copy of the ASCII files containing areal rain rates for each Julian day.

Version 1 (V1) S-POL rain maps for the LBA field campaign were completed during September 2000. Instantaneous rain map images (GIF format) such as in Fig. 6 are now available to the public at http://radarmet.atmos.colostate.edu/trmm_lba/rainlba.html . These rain rate maps were created at a temporal frequency of about once every ten minutes during the operational period of the S-POL radar (see Sec. 2 for more details). Daily and monthly rain accumulation map images, as in Figs. 7 and 8 respectively, will be made available at the same web site soon. In addition, TRMM scientists can request rain accumulation maps for any arbitrary time period lasting over 20 minutes during the LBA field campaign (e.g., specific case study time interval, weekly, 5-day, 30-day) by contacting the CSU Radar Meteorology Group.
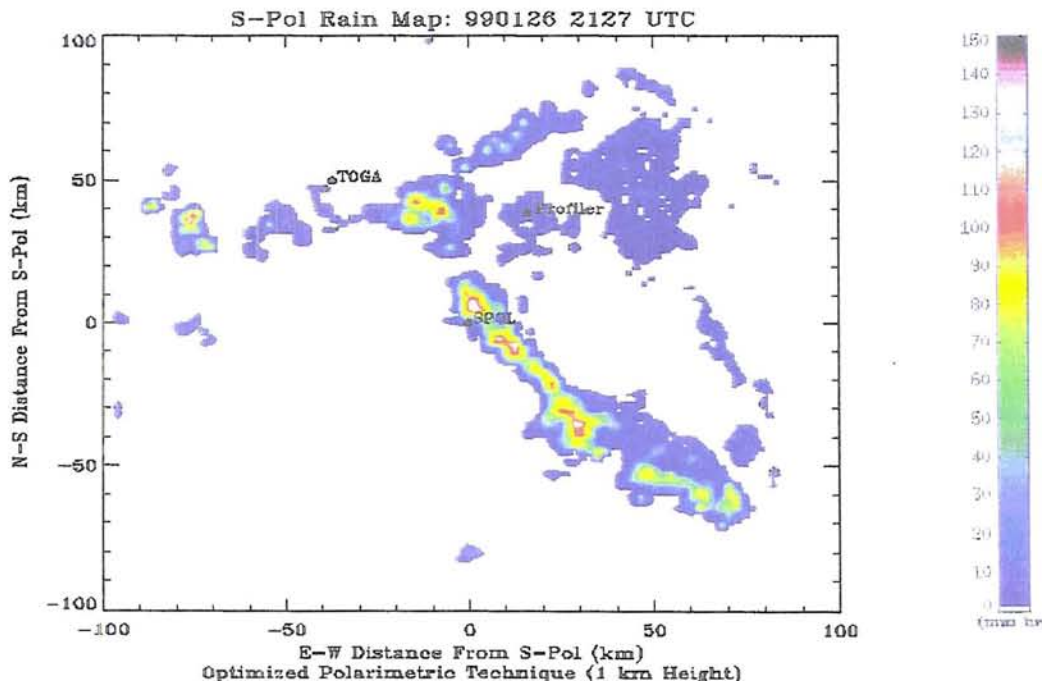

Fig. 6. Example of a S-POL V1 instantaneous rain rate (mm h^{-1}) map from the 26 January 1999 (2127 UTC) easterly regime MCS case. Instantaneous rain maps from TRMM-LBA are now available at the CSU Radar Meteorology web site.

TRMM-LBA: S-POL Rain Map
Cumulative Rain Depth (mm)
15 Feb 99

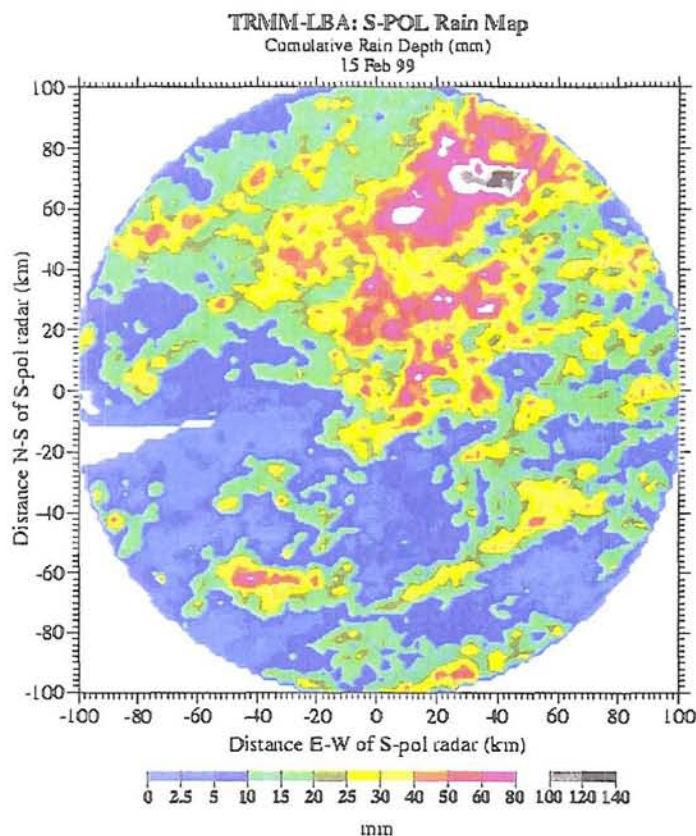0 2.5 5 10 15 20 25 30 40 50 60 80 100 120 140
mm

Fig. 7. Example of a S-POL V1 daily rain accumulation (mm) map from 15 Feb 99 (UTC), which was characterized by widespread and occasionally heavy nocturnal rain.
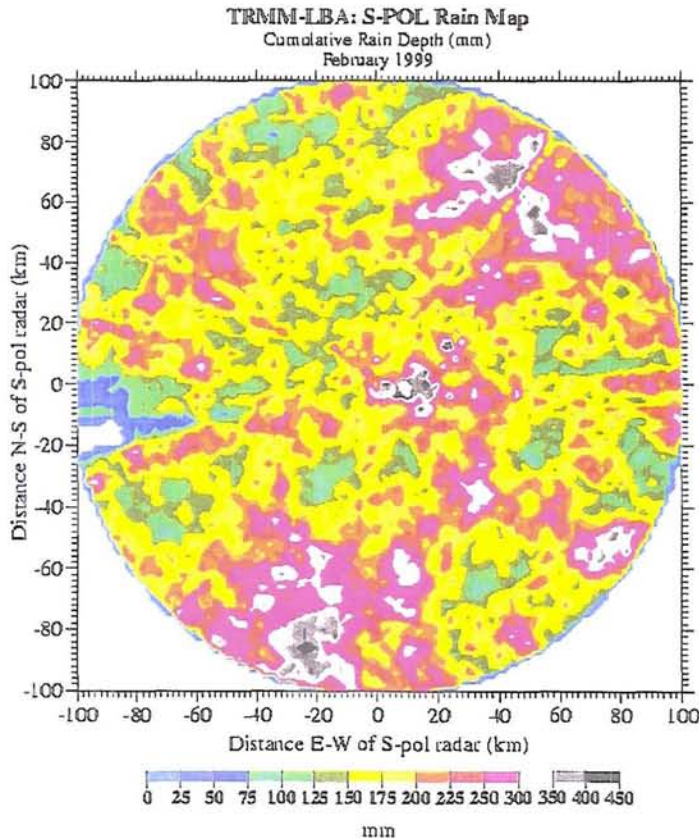

TRMM-LBA: S-POL Rain Map
Cumulative Rain Depth (mm)
February 1999

0 25 50 75 100 125 150 175 200 225 250 300 350 400 450
mm

Fig. 8. Example of a S-POL V1 monthly rain accumulation (mm) map for February 1999 (UTC) over the TRMM-LBA domain
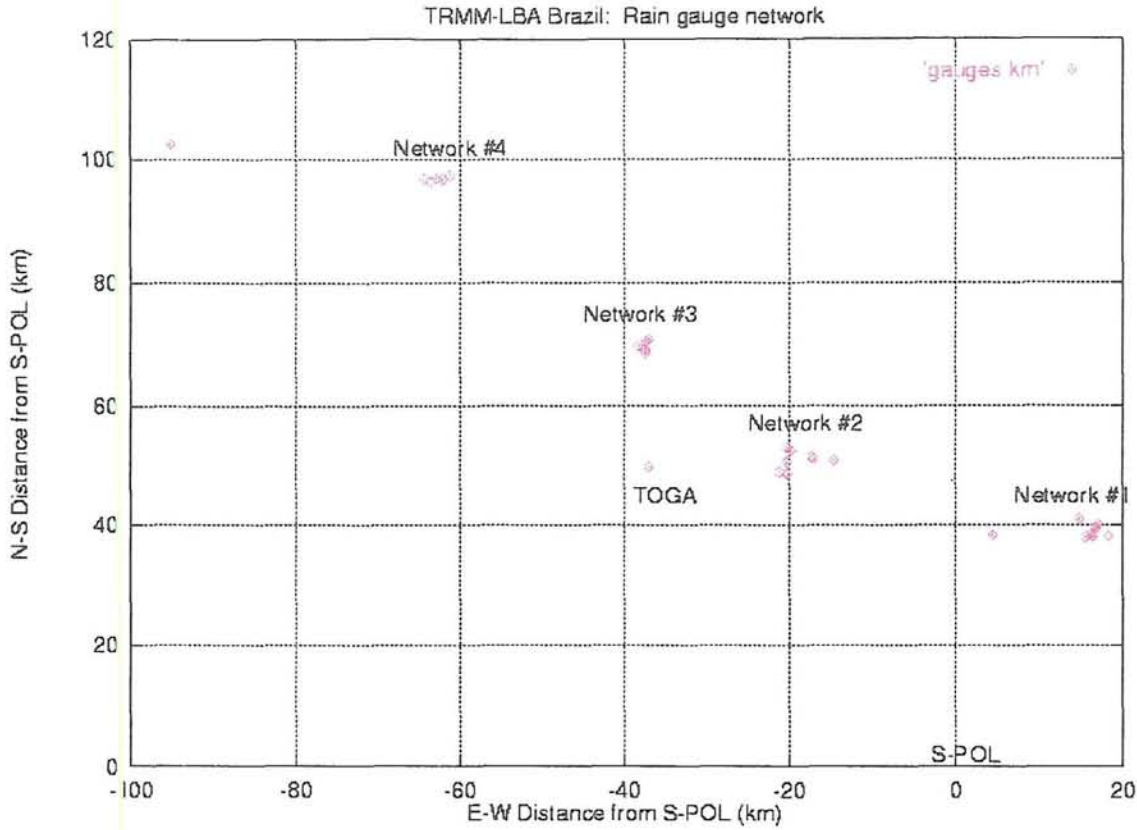
10

Fig. 9. Diagram of the rain gauge network deployed in Rondonia, Brazil for the TRMM-LBA field experiment.

b. Comparison with TRMM-LBA rain gauges

In order to evaluate and validate the V1 S-POL radar rainfall estimates, we performed a simple comparison between the gridded S-POL radar estimate of rain accumulation and the readings from 33 tipping rain gauges available within 100 km of the radar for the entire month of February 1999. The 33 rain gauges were located at the TOGA radar and rain gauge networks # 1, 2, and 3 (Fig. 9). Several of the gauges in network #3 and all of the gauges in Network #4 were excluded from the comparison because they are outside of the 100 km radius from S-POL.

Because of known issues in comparing radar and gauge estimates of rainfall, we utilized three different (yet all simple) techniques for comparing the gridded (2 km x 2 km) radar data to the gauge accumulations. First, we simply picked the grid point within a characteristic grid scale length ($\sqrt{\Delta x^2 + \Delta y^2} = 2.8\,km$) of each rain gauge that most closely matched the corresponding gauge rain total (optimal method). Second, we utilized the median S-POL rain estimate with 2.8 km of each gauge (median method). Third, we chose the S-POL rain estimate physically closest to each gauge (closest method).

Results of the S-POL-to-gauge rain total comparison are summarized in Tables 2 and 3. The S-POL radar rainfall estimate was biased low in the range of 4.8% - 11.1%. The standard error of the S-POL rain total estimate ranged from 14.4% to 20.6%. These ranges of standard error and bias for polarimetric radar-to-gauge comparisons are typical (e.g., Ryzhkov and Zrnic, 1995b;

Ryzhkov and Zrnic, 1996; Ryzhkov et al., 1997; Bolen et al., 1998; May et al., 1999; Carey et al., 2000).

Table 2. TRMM-LBA: S-POL versus gauge rainfall statistics for February 1999

Statistic	Gauges	S-POL Optimal	S-POL Median	S-POL Closest
Count	33	33	33	33
Mean	215.1 mm	204.8 mm	192.1 mm	191.3 mm
Standard Deviation	44.2 mm	25.5 mm	26.8 mm	35.8 mm
Median	224.6 mm	208.3 mm	198.8 mm	197.6 mm
Minimum	100.1 mm	143.2 mm	140.2 mm	128.0 mm
Maximum	360.5 mm	233.9 mm	225.2 mm	228.2 mm

Table 3. Performance of the S-POL rainfall estimate relative to rain gauges for February 1999

Method	NORMALIZED BIAS	NORMALIZED STANDARD ERROR
S-POL Optimal	-4.8%	14.4%
S-POL Median	-10.7%	17.9%
S-POL Closest	-11.1%	20.6%

A scatter plot of individual radar-to-gauge comparison points is depicted in Fig. 10. Note that there are two outliers out of the 33 gauges that do not compare well to the S-POL estimate. In one instance, the gauge total is nearly 100 mm lower than the S-POL estimate. In the other case, the gauge accumulation is more than 100 mm greater than the S-POL estimate. Interestingly, these two gauges were within 2 km of each other. The mean gauge total for these two outliers (230.3 mm) compares very favorably to the mean of the S-POL rain totals in the two grid points closest to the two gauges (225.8 mm). After averaging in this manner, the cumulative S-POL rain estimate for these two gauges is within 2%.
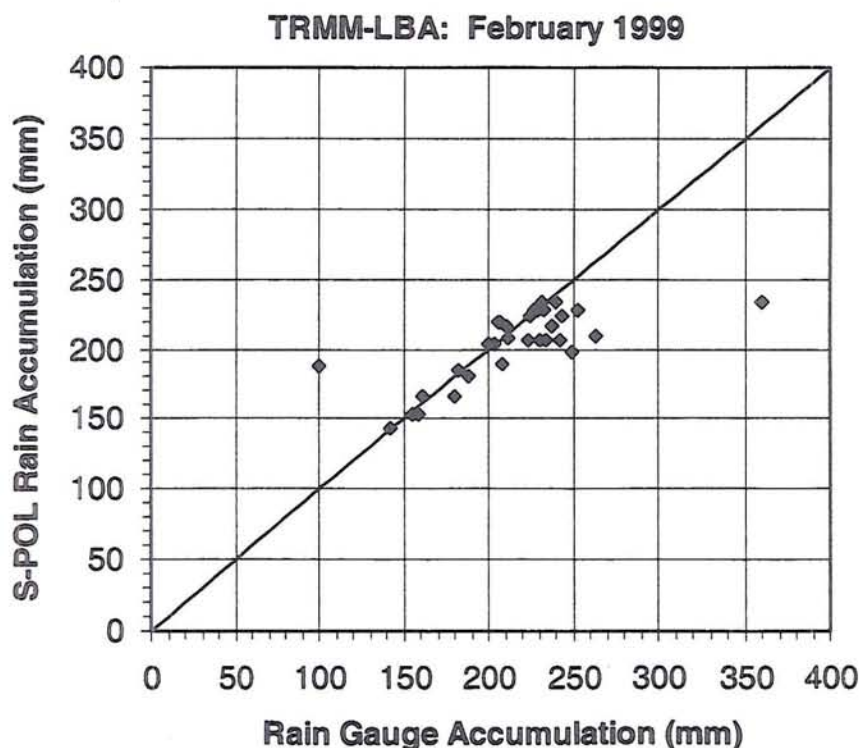
TRMM-LBA: February 1999

Fig. 10. A scatter plot of the optimal S-POL radar versus gauge total rain accumulations for February 1999.

4. Selected Preliminary Scientific Results

While quality controlling the S-POL data and creating the V1 S-POL rain maps, we have utilized the areal rain rate estimates made from S-POL differential propagation phase (ϕ_{dp}) in our scientific research. With these data, we have investigated the LBA time series of rainfall (Fig. 11), the characteristics of areal rain rate by meteorological regime (Table 4 and Fig. 12), and the diurnal cycle of rainfall by regime (Fig. 13).

When comparing the magnitude of areal rain rates calculated with the S-POL phase-based technique to other data sources, it is important to note that the areal rain rates are **unconditional** over the radar domain due to the very nature of the method. In other words, the mean areal rain rate includes non-raining areas over the radar domain.
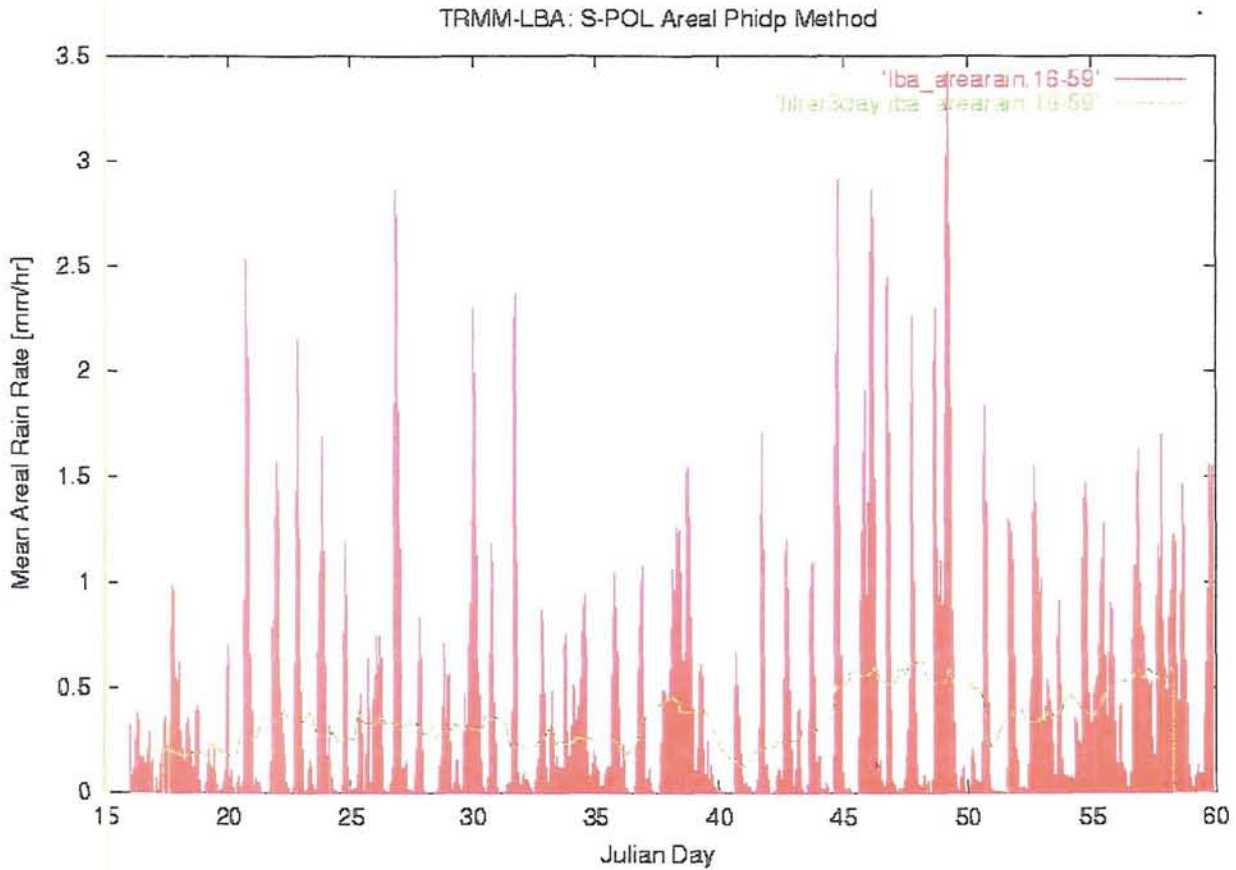

Fig. 11. Time series of S-POL (unconditional) areal rain rate (mm h⁻¹) during the TRMM-LBA experiment as determined by the differential phase method. The red impulses depict the unfiltered time series. The green line represents the 3-day filtered time series.

At the simplest level, the time series of areal rain rate in Fig. 11 demonstrates how ubiquitous rainfall is in Amazonia (see also fractional rain durations in Table 4). It is also apparent that rainfall is highly diurnally modulated. Yet there are some hints of nocturnal rainfall, which appears to be occasionally very intense. During the easterly low-level wind regime, rainfall tends to be narrowly peaked in the diurnal (e.g., JD 21 – 27 and 41 – 51). During the westerly wind regime, the areal rainfall is often more broadly peaked in the diurnal (e.g., 16 – 18, 52 –

13

60). Apparently, there are also exceptions to this general rule. The 3-day filtered areal rain rate shows several broad peaks and brief minima. Interestingly, the amplitude and period of the 3-day cycle increases as the experiment progresses. Periods of increasing 3-day filtered areal rain rate include JD 20-23, 37-38, 41-45, and 51-57. During January (February), the broad maxima and narrow minima are separated by about 5 (10) days. Detailed spectral analyses of the rain rate time series are under way.
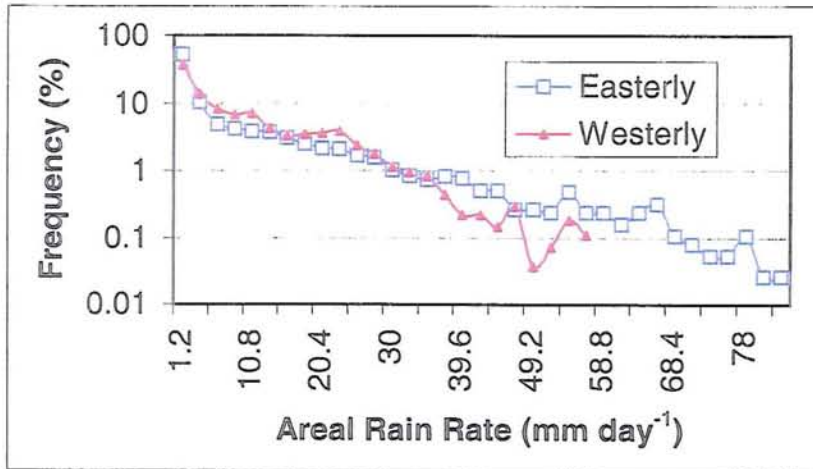

Fig. 12. Frequency histogram of the S-POL (unconditional) areal rain rate (mm day^{-1}) that is partitioned by meteorological regime.

As seen in the frequency histogram (Fig. 12) and statistical summary (Table 4) of S-POL areal rain rate, the biggest differences between the easterly and westerly regime occur in the extremes of the distribution. The easterly regime has a larger fraction (52%) of the distribution at very low rain rates ($\approx$ 1 mm day^{-1}) than the westerly regime (37%). The distribution of the easterly regime areal rain rate also possesses a long tail into large values while the westerly regime does not. As a result, the 25th percentile, median, 75th percentile and mean areal rain rate are larger for the westerly than the easterly regime. On the other hand, the 95th percentile and maximum areal rain rate are higher in the easterly regime compared to the westerly regime. Also due to the behavior in the tails, the standard deviation of the areal rain rate is larger in the easterly regime. The fractional duration is noticeably higher at low-to-moderate areal rain rates (0 - 10 mm day^{-1}) in the westerly regime. Conversely, the fractional duration of heavy areal rain (50 mm day^{-1}) is significantly larger in the easterly regime. Even though the S-POL radar undersampled the westerly regime, the measured mean areal rain depth is still larger in the westerly regime.

Fig. 13 clearly demonstrates the highly peaked diurnal nature of convection over Amazonia. Daily solar insolation is clearly a primary control over rainfall with a rapid increase in convective development and associated rainfall from late morning (11 am) to early afternoon (1 pm). However, nocturnal systems did occur on occasion. A secondary peak in the areal rainfall is present at about 1 am with local minima in rainfall at 10 am and 10 pm. The amplitude of the diurnal cycle is larger in the easterly regime. The nocturnal maximum is largely absent in the westerly regime. Also, the daytime peak is two hours later in the easterly regime (3pm) compared to the westerly regime (1pm with a hint of secondary maxima at 4 and 8 pm).

Table 4.
Areal Rain Rate Statistics from S-POL ϕ_{dp}
TRMM-LBA 10 Jan 99– 28 Feb 99

|	ALL	EASTERLY	WESTERLY
Mean (mm day^{-1})	8.5	8.4	8.7
Minimum (mm day^{-1})	0.0	0.0	0.0
Maximum (mm day^{-1})	82.1	82.1	56.9
Std. Deviation (mm day^{-1})	12.0	13.2	9.9
95th Percentile (mm day^{-1})	33.0	37.1	28.4
75th Percentile (mm day^{-1})	12.5	11.8	13.1
Median (mm day^{-1})	3.0	2.0	4.6
25th Percentile (mm day^{-1})	0.4	0.2	1.1
Depth (mm)	481.6	227.8	252.8
Fractional Duration R > 0 mm day^{-1} (%)	87.9	84.4	92.8
Fractional Duration R > 1 mm day^{-1} (%)	67.0	60.6	75.9
Fractional Duration R > 10 mm day^{-1} (%)	30.1	27.8	33.4
Fractional Duration R > 50 mm day^{-1} (%)	1.6	2.5	0.4
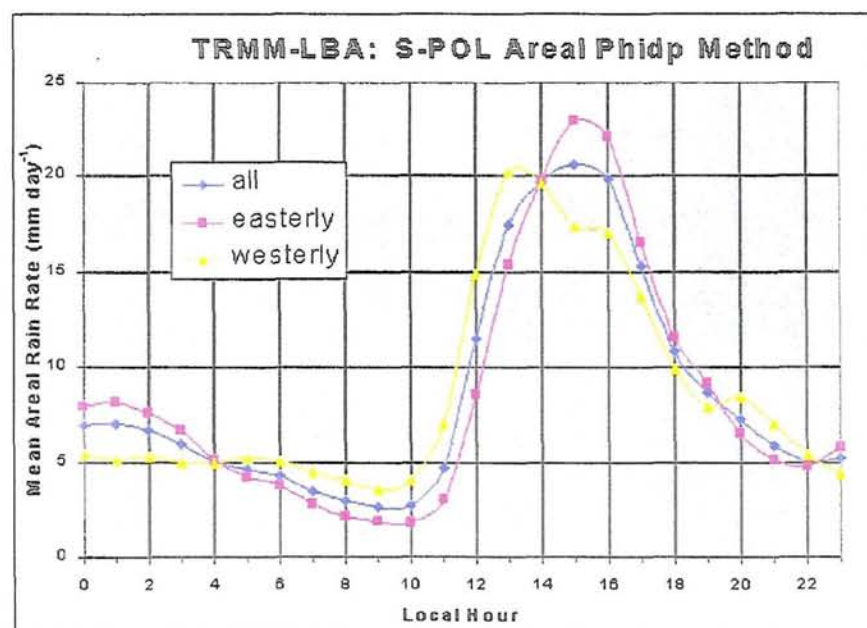
Fig. 13. S POL (unconditional) areal rain rate (mm day^{-1}) versus time (local hour). The plot depicts the composite diurnal cycle of (unconditional) areal rain rate over the S-POL TRMM-LBA domain during the entire experiment (all), during easterly low-level winds regime (easterly), and during westerly low-level wind regime (westerly).

15

5. Plans for Version 2 (V2) S-POL Rainfall Maps and Associated Science

a. Version 2 Improvements

Although we consider the performance (5% to 11% negative bias and 14% to 21% standard error relative to the gauges) of the V1 S-POL monthly rain maps to be exemplary and consistent with prior polarimetric radar studies, there are still opportunities for improvement. Here is a bulleted list of our intended improvements for the Version 2 rain map effort, which should be complete before January 2001.

- *Further Ground Clutter Reduction*: As can be seen in Fig. 8, some ground clutter east of the radar is still passing through the polarimetric thresholding procedures outlined in Sec. 2a. We plan to run sensitivity tests on the efficacy of various thresholds for ρ_{hv} and $\sigma[\phi_{dp}]$ in reducing the ground clutter. We hope that these sensitivity tests will result in thresholds that provide more effective clutter rejection. In addition, we will explore the combination of traditional Doppler spectral and polarimetric techniques in further reducing the impact of ground clutter. If we are unable to improve the clutter rejection in these small areas near the radar to our satisfaction, we will mask them out of the V2 rainfall estimates.

- *Partial and Near Complete Beam Blocking*: As can be seen in Figs. 7 and 8, there are azimuthal artifacts in select quadrants (e.g., WSW) of the daily and monthly rainfall totals. Given the near complete blocking in the lowest elevation angles (0.7° and 1.1°) at these azimuths (see Figs. 3ab), this is not too surprising. When near complete blocking occurs, only very intense echoes produce a signal back at the radar that is above the minimum detectable power such that a phase measurement is made. Hence, many weak-to-moderate cells are missed at these azimuths to the WSW. In addition, a few rays to the WSW are completely blocked at the lowest tilt. In these rays that are either completely blocked or nearly all blocked, we will set all data to the bad data flag and effectively mask out the sector. Only a few rays (e.g., up to a 5° sector to the WSW) should be masked out in this fashion. We will also look at improving our ΔZ_h correction for partial blocking.

- *Bias Reduction*: Since the -5% to -11% bias is relatively small, it may *not* be possible to objectively improve upon V1 in this matter. There are many possible causes for this negative bias, including the typical explanations such as differing spatial resolutions and the effect of smoothing on radar data. For polarimetric applications, there is one dominant assumption in the development of rain rate equations that could be causing a bias in our results. The key assumption is the drop shape versus drop diameter relationship. In many past studies, the Pruppacher and Beard (1970) relationship was used and rainfall rates were typically biased by 10% to 30% too low. We chose the rain rate relationships of Bringi and Chandrasekar (2000), who utilized the Beard and Chuang (1987) equilibrium drop shape versus size equation, which results in drops that are less oblate for a given size than the wind tunnel studies of Pruppacher and Beard (1970). If all else is equal, less oblateness in raindrops results in higher rain rates for the same

polarimetric measurements. Recent studies by Andsager et al. (1999) and Keenan et al. (2000) suggest that rain drops in real clouds may be even less oblate for a given size than is suggested by the equilibrium relationship of Beard and Chuang (1987). We will explore using the oblateness relationship of Andsager et al. (1999) in the development of our V2 rain rate relationships. It may be that an incorrect oblateness versus size relationship is the primary physical explanation for the remaining -10% bias in our rain totals.

b. Future Science Plans

Once the V2 S-POL radar rainmaps are complete, we intend to research a host of scientific questions associated with TRMM-LBA. Here are some issues that we plan to explore in collaboration with other TRMM scientists:

- The relationship between rainfall statistics and large-scale meteorological regime, including spectral analyses of the rainfall time series data
- The creation of regime ensemble rain rate, in-cloud rain mass, mixed phase ice mass, divergence, vertical velocity, and mass flux statistics
- The partitioning of rainfall statistics by storm size, morphology, and duration
- The association between the rain depth at a grid point and the PDF of rain rate and rain duration
- The connection between land surface properties in Amazonia (deforested/pasture versus forest canopy) to rainfall amounts and characteristics
- The polarimetric tuning (e.g., Ryzhkov et al., 1997) of the Z-R relationship(s) used by the TOGA radar in the creation of rainmaps for TRMM-LBA.
- The validation of the TRMM satellite rainfall algorithms over the LBA domain.

REFERENCES

Andsager, K., K. V. Beard, and N. F. Laird, 1999: Laboratory measurements of axis ratios for large raindrops. *J. Atmos. Sci.*, **56**, 2673-2683.

Beard, K. V., and C. Chuang, 1987: New model for the equilibrium shape of raindrops. *J. Atmos. Sci.*, **44**, 1509-1524.

Bolen, S., V. N. Bringi, and V. Chandrasekar, 1998: An optimal area approach to intercomparing polarimetric radar rain-rate algorithms with gauge data. *J. Atmos. Oceanic Technol.*, **15**, 605-623.

Bringi, V. N., V. Chandrasekar, N. Balakrishnan, and D. S. Zrnic, 1990: An examination of propagation effects in rainfall on radar measurements at microwave frequencies. *J. Atmos. Oceanic Technol.*, **7**, 829-840.

Bringi, V. N., and V. Chandrasekar, 2000: Polarimetric Doppler Weather Radar-Principles and Applications, in press.

Carey, L. D., and S. A. Rutledge, 1998: Electrical and multiparameter radar observations of a severe hailstorm. *J. Geophys. Res.*, **103**, 13,979-14,000.

Carey, L. D., and S. A. Rutledge, 2000: The relationship between precipitation and lightning in tropical island convection: A C-band polarimetric radar study. *Mon. Wea. Rev.*, **128**, 2687-2710.

Carey, L. D., S. A. Rutledge, D. A. Ahijevych, and T. D. Keenan, 2000: Correcting propagation effects in C-band polarimetric radar observations of tropical convection using differential propagation phase. *J. Appl. Meteor.*, **39**, 1405-1433.

Chandrasekar, V., E. Gorgucci, and G. Scarchilli, 1993: Optimization of multiparameter radar estimates of rainfall *J. Appl. Meteor.*, **32**, 1288-1293.

Jameson, A. R., 1991: A comparison of microwave techniques for measuring rainfall. *J. Appl. Meteor.*, **30**, 32-54.

Keenan, T. D., L. D. Carey, D. S. Zrnic, and P. T. May, 2000: Sensitivity of 5-cm wavelength polarimetric radar variables to raindrop axial ratio and drop size distribution. *J. Appl. Meteor.*, in press.

May, P. T., T. D. Keenan, D. S. Zrnic, L. D. Carey, and S. A. Rutledge, 1999: Polarimetric radar measurements of tropical rain at a 5-cm wavelength. *J. Appl. Meteor.*, **38**, 750-765.

Petersen, W. A., L. D. Carey, S. A. Rutledge, J. C. Knievel, N. J. Doesken, R. H. Johnson, T. B. McKee, T. Vonder Haar, J. F. Weaver, 1999: Mesoscale and radar observations of the Fort Collins Flash Flood of 28 July 1997, *Bull. Amer. Meteorol. Soc.*, **80**, 191-216.

Pruppacher, H. R., and K. V. Beard, 1970: A wind tunnel investigation of the internal circulation and shape of water drops falling at terminal velocity in air. *Quart. J. Roy. Meteor. Soc.*, **96**, 247-256.

Ryzhkov, A. V., D. S. Zrnic, 1995a: Precipitation and attenuation measurements at a 10-cm wavelength. *J. Appl. Meteor.*, **34**, 2121-2134.

Ryzhkov, A. V., D. S. Zrnic, 1995b: Comparison of dual-polarization radar estimators of rain. J. Atmos. Oceanic Technol., **12**, 249-256.

Ryzhkov, A. V., D. S. Zrnic, 1996: Assessment of rainfall measurement that uses specific differential phase. *J. Appl. Meteor.*, **35**, 2080-2090.

Ryzhkov, A. V., D. S. Zrnic, and D. Atlas, 1997: Polarimetrically tuned R(Z) relations and comparisons of radar rainfall methods. *J. Appl. Meteor.*, **36**, 340-349.

Ryzhkov, A. V., and D. S. Zrnic, 1998: Polarimetric rainfall estimation in the presence of anomalous propagation. *J. Atmos. Oceanic Technol.*, **15**, 1320-1330.

Ryzhkov, A. V., D. S. Zrnic, 2000: Areal rainfall estimates using differential phase. *J. Appl. Meteor.*, **39**, 263-268.

Scarchilli, G., E. Gorgucci, V. Chandrasekar, and A. Dobaie, 1996: Self-consistency of polarization diversity measurements of rainfall. *IEEE Trans. On Geo. and Rem. Sen.*, **34**, 22-26.

Zrnic, D. S., and Ryzhkov, A. V., 1999: Polarimetry for weather surveillance radars. *Bull. Amer. Meteorol. Soc.*, **80**, 389-486.